Acta Crystallographica Section B
Structural Science
ISSN 0108-7681

Re-investigation of the structure and crystal chemistry of the Bi_2O_3–W_2O_6 'type (Ib)' solid solution using single-crystal neutron and synchrotron X-ray diffraction

Neeraj Sharma,[a]* Rene B. Macquart,[b] Maxim Avdeev,[a] Mogens Christensen,[c] Garry J. McIntyre,[d] Yu-Sheng Chen[e] and Chris D. Ling[a,b]

[a]Bragg Institute, Australian Nuclear Science and Technology Organization, PMB 1, Menai, NSW 2234, Australia, [b]School of Chemistry, The University of Sydney, Sydney, NSW 2006, Australia, [c]Department of Chemistry, University of Aarhus, DK-8000 Aarhus C, Denmark, [d]Institut Laue–Langevin, 6 rue Jules Horowitz, BP 156, 38042 Grenoble CEDEX 9, France, and [e]ChemMatCars, Advanced Photon Source, Argonne National Laboratories, Argonne, IL 60439, USA

Correspondence e-mail: njs@ansto.gov.au

Received 6 November 2009
Accepted 14 January 2010

Single crystals of composition $Bi_{35.66}W_{4.34}O_{66.51}$ (or $Bi_{8.2}WO_{15.3}$, bismuth tungsten oxide), within the type (Ib) solid-solution region of the Bi_2O_3–WO_3 system, were synthesized using the floating-zone furnace method. Synchrotron X-ray and neutron single-crystal diffraction data were used to confirm the previously tentative assignment of the room-temperature space group as $I4_1$. Fourier analysis of the combined X-ray and neutron datasets was used to elucidate and refine fully the cation and anion arrays for the first time. The mixed cation site $M1$ is shown to be coordinated by eight O atoms in an irregular cube when M = Bi, and by six O atoms in an octahedron when M = W. The resulting disorder in the average structure around $M1$ is discussed in the context of experimentally observed oxide-ion conductivity.

1. Introduction

The high-temperature polymorph of bismuth oxide, δ-Bi_2O_3, features high oxide-ion conductivity at temperatures around 1023 K (Sammes *et al.*, 1999). δ-Bi_2O_3 has a fluorite-type (CaF_2) structure with cubic symmetry and average oxygen occupancy of 75% (Gattow & Schröder, 1962). Oxide-ion conductivity in δ-Bi_2O_3 is related to the presence of 25% oxide-ion vacancies and the high polarizability of the cation network afforded by Bi^{3+} ions with their $6s^2$ lone pair of electrons (Boivin & Mairesse, 1998). Unfortunately, δ-Bi_2O_3 is only stable at temperatures above 1003 K, limiting its use as an ionic conductor. In order to stabilize the δ-Bi_2O_3 structure type down to room temperature, transition-metal dopants such as Nb^{5+}, Ta^{5+}, Cr^{6+}, Mo^{6+}, W^{6+} and Re^{7+} (Crumpton *et al.*, 2005; Cheetham & Rae Smith, 1985: Liu *et al.*, 2008; Ling *et al.*, 1998; Sharma *et al.*, 2009) may be introduced, producing a variety of complex modulated structures (or superstructures) based on the fluorite-type subcell. These Bi-rich transition-metal-doped δ-Bi_2O_3 structures, including many W^{6+}-doped examples, show similar oxide-ion conductivities to that shown by pure δ-Bi_2O_3 at elevated temperatures (Watanabe & Ono, 2004; Takahashi & Iwahara, 1973; Sammes *et al.*, 1999).

Work on the Bi-rich end of the Bi_2O_3–W_2O_6 pseudo binary system (Fig. 1) has revealed a partially disordered phase at $Bi_{14}WO_{24}$ (Ling, 2006; Crumpton *et al.*, 2003; Spinolo & Tomasi, 1997; Ling *et al.*, 1999), an oxygen deficient phase at $Bi_7WO_{13.5}$ (Nespolo *et al.*, 2002; Watanabe *et al.*, 1985; Watanabe & Ono, 2004), and an Aurivillius-type phase Bi_2WO_6 (McDowell *et al.*, 2006; Rae *et al.*, 1991; Wolfe *et al.*, 1969; Takahashi & Iwahara, 1973). With one exception, all other fluorite-related phases with Bi:W ratios between 30:1 and 2:1 have been shown to fall into solid-solution regions described for the above-mentioned phases by Zhou (1994), Hoda & Chang (1974) and Ling *et al.* (1998). The only exception is a

solid-solution region located around $Bi_{4.5}WO_{9.75}$, described by Zhou (1994) as type (II), but this was never isolated as a single phase and no further work was carried out.

At the Bi-rich end of the Bi_2O_3–W_2O_6 phase diagram, $Bi_{14}WO_{24}$ (Ling, 2006; Crumpton *et al.*, 2003; Spinolo & Tomasi, 1997; Ling *et al.*, 1999) contains isolated WO_4 units in a fluorite-type matrix. Increasing W_2O_6 content results in the solid-solution phase $Bi_2O_3{\cdot}xW_2O_6$, $0.08 \lesssim x \lesssim 0.19$, first labeled as type (Ib) by Zhou (1994). The type (Ib) phase of composition $Bi_7WO_{13.5}$ (Nespolo *et al.*, 2002; Watanabe *et al.*, 1985; Watanabe & Ono, 2004) was shown to have similar cation arrangements to $Bi_{14}WO_{24}$ with a modified periodicity of W-containing planes (Zhou, 1994). Initially it was modeled in the space group $I4_1/a$ (Watanabe *et al.*, 1985) before the *a*-glide plane was found to be weakly broken, reducing the symmetry to $I4_1$ with cell parameters a = 12.513 (2) and c = 11.231 (4) Å (Nespolo *et al.*, 2002). The relationship between the unit cell of type (Ib) and that of fluorite-type δ-Bi_2O_3 is $\mathbf{a} = 2\mathbf{a}_f + \mathbf{b}_f$, $\mathbf{b} = -\mathbf{a}_f + 2\mathbf{b}_f$ and $\mathbf{c} = 2\mathbf{c}_f$.

Full structural characterization of the type (Ib) solid-solution phases has been extremely difficult because only small twinned crystals have been available, and because the structure contains crystallographic sites with mixed-cation occupancy. As Bi^{3+} and W^{6+} have very different preferred coordination environments in oxides, crystallographic sites with mixed cation occupancy imply significant associated disorder in the average oxygen sublattice. Such disorder is beneficial for oxide-ion conductivity (Francesconi *et al.*, 1998), but difficult to treat crystallographically. A particular challenge faced by earlier X-ray diffraction-based studies has been the similarity of the X-ray scattering powers of Bi and W (with 83 and 74 electrons, respectively) and that both are much stronger than the X-ray scattering power of O. Consequently, while previous studies have been able to compare different chemically reasonable models for the structure of the type (Ib) phase by testing them against X-ray diffraction data, they have not been able to actually refine those models.

In this work we have investigated a crystal in the type (Ib) solid solution with a combination of single-crystal synchrotron X-ray diffraction and single-crystal neutron diffraction. Neutron diffraction has the advantage of greater contrast between Bi and W (scattering lengths $b_{coherent}$ of 8.532 and 4.86 fm) and greater sensitivity to O ($b_{coherent}$ of 5.803 fm) in the presence of Bi and W, compared with X-ray diffraction. This sensitivity has allowed us to carry out full crystallographic refinements of the type (Ib) phase for the first time.

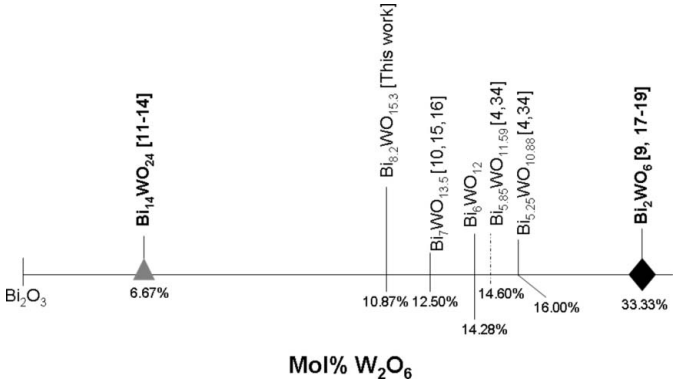

Figure 1
Partial phase diagram of the pseudo-binary Bi_2O_3–W_2O_6 system at room temperature showing tetrahedrally coordinated W phases with gray triangles and octahedrally coordinated W phases with black diamonds. Full crystallographic refinements have been reported for the compounds in bold font. The phase at 14.28% W_2O_6 represents the W-rich limit of the type (Ib) solid solution with octahedrally coordinated W in $I4_1$. The phase with the dotted line has been interpreted with a W oxidation state of 5.63+.

2. Experimental

Bi_2O_3 (5N Sigma Aldrich) and WO_3 (4N Fluka) mixtures in the formula proportion 3.42:1 were ground in a planetary ball mill for 70 h with ethanol added to facilitate homogenous grinding, then samples were heated at 1103 K for 3 h. Rods of the samples were pressed at 60 MPa and sintered at 1103 K for 1 h in a vertical tube furnace. These rods were then mounted in an optical floating zone furnace (Crystal Systems Corporation Model FZ-T-10000-H-VI-VPM-PC) with 300 W filaments. The rods melted between 36 and 38% power and were taken through the hot zone at rates of 1–10 mm h^{-1} with rotation speeds of 10–30 r.p.m.

Approximate Bi:W ratios in the grown rods were found to be 6.1 (3):1 by energy-dispersive X-ray spectroscopy (EDS) using a Philips XL30 scanning electron microscope (SEM). The EDS-determined Bi:W ratio was slightly lower than the input Bi:W ratio of 6.84:1. As Bi_2O_3 has a high vapor pressure, we expected the final Bi:W ratio of grown crystals to be slightly different from the input ratio. The 6 mm diameter synthesized rods were found to be coarsely polycrystalline, with single-crystalline grains of up to $\sim$ 12 mm^3. Crystals were initially analyzed on a Bruker–Nonius APEX-II X-ray diffractometer with Mo $K\alpha$ radiation (λ = 0.71073 Å).

Single-crystal neutron diffraction data were collected on the very intense vertical-axis Laue diffractometer (VIVALDI) at the Institut Laue–Langevin (ILL), Grenoble, France (McIntyre *et al.*, 2006; Wilkinson *et al.*, 2002). VIVALDI uses a polychromatic ('white') neutron beam from a thermal guide ($0.8 \leq \lambda \leq 5.2$ Å) with a cylindrical image-plate detector. A $\sim$ 12 mm^3 crystal was mounted on a vanadium pin with epoxy, placed in the neutron beam and exposed for 30 min per Laue pattern. Sixteen patterns were collected, separated by 14° rotations perpendicular to the neutron beam in order to obtain good data redundancy and completeness. Reflections were indexed using the program *LAUEGEN* (Campbell *et al.*, 1998; Campbell, 1995), integrated using ARGONNE_BOXES (Wilkinson *et al.*, 1988), and normalized to the wavelength distribution of the white neutron beam using LAUENORM (Campbell *et al.*, 1986). Note that when carrying out refinements against white-beam neutron data, equivalent reflections must not be merged prior to refinement; this is because they generally result from the diffraction of different wavelength neutrons, and are therefore subject to different extinction effects.

Table 1
Final refined fractional atomic coordinates, atomic displacement parameters, and bond-valence sums (BVS) for $Bi_{35.66}W_{4.34}O_{66.51}$ (or $Bi_{8.2}WO_{15.3}$).

Equivalent isotropic atomic displacement parameters are given for metal atoms. Positions, atomic displacement parameters and occupancies are determined from simultaneous refinement against neutron and synchrotron X-ray diffraction data. Occupancies for the corresponding sites of type (Ib) phases reported in the literature are given.

Atom	Wyckoff position	*x*	*y*	*z*	U_{eq}/U_{iso}	BVS	Fractional occupancy	$Bi_{5.85}WO_{11.8}$ (Ling, 1999) Occ. for equivalent sites	$Bi_7WO_{13.5}$ (Nespolo *et al.*, 2002) Occ. for equivalent sites
*M*1	4*a*	0.5	0.5	0.5	0.0389 (6)	2.49	0.91 (6) Bi	0.54 Bi	1 Bi
(W1)				[0.473 (3)†]		5.94	0.085 (6) W	0.46 W	
*M*2	4*a*	0.5	0.0	0.2460 (5)‡	0.0130 (5)	5.94	1 W	1 W	1 W
*M*3*a*	8*b*	0.2922 (1)	0.1057 (1)	0.9826 (4)	0.0225 (5)	2.15	1 Bi	1 Bi	0.875 Bi
									0.125 W
*M*3*b*	8*b*	0.7096 (2)	0.3936 (1)	0.2755 (4)	0.0288 (5)	3.10	1 Bi	1 Bi	1 Bi
*M*4*a*	8*b*	0.2047 (2)	0.3957 (1)	0.0078 (4)	0.0264 (5)	3.18	1 Bi	1 Bi	1 Bi
*M*4*b*	8*b*	0.7958 (2)	0.1026 (1)	0.2445 (4)	0.0251 (4)	3.36	1 Bi	1 Bi	1 Bi
O1*a*	8*b*	0.1221 (7)	0.0407 (7)	0.0884 (9)	0.0224 (5)§	2.27	0.314¶	1	0.6
O1*b*	8*b*	0.8462 (2)	0.4335 (3)	0.1506 (5)	0.0224 (5)§	1.74	0.915 (6)††	1	1.0
O2*a*	8*b*	0.0662 (3)	0.3123 (2)	0.0735 (5)	0.0224 (5)§	2.14	0.915 (6)††	1	1.0
O2*b*	8*b*	0.9393 (3)	0.1563 (3)	0.1524 (5)	0.0224 (5)§	2.02	0.915 (6)††	1	1.0
O1*a*1	8*b*	0.5082†	0.3922†	0.594 (3)†	0.112 (18)§	2.34	0.085 (6)‡‡	–	–
O1*b*1	8*b*	0.5082†	0.3922†	0.352 (3)†	0.112 (18)§	2.84	0.085 (6)‡‡	–	–
O2*b*1	8*b*	0.3475†	0.4884†	0.473 (3)†	0.112 (18)§	2.94	0.085 (6)‡‡	–	–
O3*a*	8*b*	0.2670 (3)	0.2787 (3)	0.1312 (6)	0.0349 (9)	2.16	1	1	1.0
O3*b*	8*b*	0.7348 (3)	0.2146 (4)	0.1104 (6)	0.0384 (10)	2.21	1	1	1.0
O4*a*	8*b*	0.3899‡	0.1060‡	0.2460 (5)‡	0.371 (7)§	2.44	1	0.46	0.6
O4*b*	8*b*	0.5750‡	0.0779‡	0.3664 (5)‡	0.371 (7)§	2.34	1	1	1.0
O5*a*	8*b*	0.5750‡	0.0779‡	0.1255 (5)‡	0.371 (7)§	2.75	1	0.46	1.0
O5*b*	8*b*	–	–	–	–	–	0	0.54	0.24

† Held as an octahedral unit with a refined rotation of $\varphi = 4.4\ (17)^\circ$ and translation of *z* refined resulting in values and errors obtained for the *z* parameter. ‡ Held as an octahedral unit with a refined rotation of $\varphi = 26.4\ (5)^\circ$ and translation of *z* refined resulting in values and errors obtained for the *z* parameter. § Atomic displacement parameters constrained to be equal. ¶ O vacancy located on this site, occupancy adjusted to satisfy the charge balance. †† Occupancies constrained to Bi content on the *M*1 site. ‡‡ Occupancies constrained to W content on the *M*1 site

The same crystal measured on VIVALDI was broken into smaller fragments, and a small ($\sim 125\ \mu m^3$) one selected for synchrotron X-ray data collection on beamline ID-15-C at the Advanced Photon Source, Argonne National Laboratories. Data were collected at 298 K at a wavelength of 0.41328 Å on a Bruker APEX-II detector. Integration of the collected data was performed with *SAINT-Plus* (Bruker AXS, 2001*b*) and a *SADABS* (Bruker AXS, 2001*a*) absorption correction was applied. Using the same crystal for both neutron and synchrotron X-ray diffraction ensured that the Bi:W ratio was the same.

Initial structural refinements were carried out with the *SHELX*97 package (Sheldrick, 2008) on the *WinGX* (Farrugia, 1999) front end. Simultaneous refinements against neutron and X-ray diffraction data were carried out using the *JANA*2006 package (Petricek *et al.*, 2007).

3. Results and discussion

3.1. Crystal chemistry

Systematic extinctions in both synchrotron X-ray and neutron diffraction data confirmed tetragonal $I4_1$ space-group symmetry. Single-crystal synchrotron X-ray diffraction data were used to determine the room-temperature lattice parameters as $a = 12.5576\ (4)$, $c = 11.2740\ (7)$ Å. As discussed in §1, the space group and unit cell still require mixed Bi/W sites and associated oxygen sublattice disorder, making a direct solution of the structure from crystallographic data extremely difficult. Therefore, we first need to consider charge-balance and crystal-chemistry requirements in order to constrain our interpretation of these data to plausible cation- and anion-ordering schemes.

In the type (Ib) solid solution, which is based on fluorite-type δ-Bi_2O_3 containing 25% oxygen vacancies, Bi^{3+} is replaced by W^{6+}. This reduces the total number of oxygen vacancies due to charge-balance requirements. Furthermore, W^{6+} sites cannot support the eightfold cubic oxygen coordination environments found in the average fluorite type. Thus, each W^{6+} site is expected to show either sixfold octahedral coordination to oxygen, requiring two oxygen vacancies in the fluorite-type lattice, or fourfold tetrahedral coordination to oxygen, requiring four oxygen vacancies in the fluorite-type lattice. Therefore, the upper limit for W^{6+} doping in fluorite-type δ-Bi_2O_3 is either $Bi_{10}WO_{18}\square_4$ (if all W^{6+} sites have tetrahedral coordination) or $Bi_6WO_{12}\square_2$ (if all W^{6+} sites have octahedral coordination), where $\square$ represents oxygen vacancies in the fluorite-type lattice. Note that both tetrahedral and octahedral W^{6+} coordinations are compatible with $I4_1$ symmetry. The fact that the reported range of W^{6+} doping for type (Ib) exceeds both these limits could be explained by the flux growth of Bi-rich crystals from a relatively W-rich melt in the two-phase region between type (Ib) and Bi_2WO_6. Nevertheless, the high reported upper limit makes octahedral coordination more likely in type (Ib). This is consistent with the report of Zhou (1994) that Raman spectroscopy shows octahedral W^{6+} coordination in type (Ib), and the exclusive presence of octahedral W^{6+} in Bi_2WO_6.

A fully ordered model for type (Ib) based on WO_6 octahedra in $I4_1$ can only be built at the composition $Bi_9WO_{16.5}$. All other compositions within the solid-solution range require mixed cation sites. Mixed Bi:W sites make structure solution extremely difficult, because Bi will have an approximately cubic coordination while W on the same site will have a regular octahedral coordination. Crystallographically, this results in 8 + 6 = 14 partially occupied O sites surrounding one mixed metal site.

3.2. Structural modelling and refinements

We label atomic sites to be consistent with the model used by Nespolo *et al.* (2002) (*M*1–*M*4*b* and O1*a*–O5*a*). The first question that must be addressed is the location of the W sites within the cation array. Previous studies agree that the 4*a* *M*2 site is fully occupied by W, but assign the mixed Bi:W site to either the 4*a* *M*1 site (Zhou, 1994; Ling, 1999; Ling *et al.*, 1998) or the 8*b* *M*3*a* site (Nespolo *et al.*, 2002; Watanabe *et al.*, 1985; Table 1). The starting model used in this study was a cation array composed exclusively of Bi sites in their ideal fluorite-type positions, and no anions. Initial refinements were carried out against synchrotron X-ray data alone, which are dominated by scattering from the cation array. As expected, refinement of the positional parameters of the cation array showed little movement away from the ideal fluorite-type positions. Replacing the *M*2 site with W improved the refinement. With *M*2 = W, occupancies of the remaining Bi sites were refined, while constraining the atomic displacement parameters of all cations to be equal. The *M*1 site occupancy decreased. Atomic displacement parameters of the cation sites were then refined, while holding them at 100% occupancy. *M*1 was the only site with an unreasonable negative atomic displacement parameter. X-ray data therefore support the assignment of the mixed site to *M*1.

We then independently used neutron Laue diffraction data to determine the cation array. In neutron diffraction the coherent scattering cross section of W is approximately half that of Bi. The same results were obtained as for X-ray data: for the *M*1 site, occupancies refined below one when atomic displacement parameters were held constant; while unrealistic atomic displacement parameters were obtained for *M*1 when the occupancies were held constant. The sensitivity of neutrons to O atoms allowed us to seek further evidence for this cation-ordering scheme by investigating the anion array. In Fourier-difference maps strong isotropic peaks were observed at all fluorite-type anion positions, except in the regions surrounding the *M*1 and *M*2 cation sites. In these areas the Fourier maps were much less clear, with anisotropic peaks around *M*1 and weaker intensity around *M*2. Neutron diffraction data therefore also support the assignment of the mixed site to *M*1.

Initial refinements of the Bi:W ratio were then undertaken with positions and atomic displacement parameters (isotropic atomic displacement parameters were used for *M*1) refining on the cation sites. Using only single-crystal neutron diffraction data, the Bi:W ratio refined to 7.86:1; using X-ray and neutron diffraction data simultaneously, it refined to 7.98:1. Then a fluorite-type anion array was progressively introduced into the simultaneous refinements, again labeled (O1*a*–O5*a*) to be consistent with the model of Nespolo *et al.* (2002) (Table 1). As a first step, the fluorite-related O sites that bond exclusively to Bi sites (O3*a*, O3*b*) were introduced and their positions and isotropic atomic displacement parameters refined. O atoms bonded to the fully occupied W site (W2) were then located using Fourier analysis. These O atoms (O4*a*–O5*a*) had weaker and broader Fourier peaks compared with the fluorite-type O atoms, and their isotropic atomic displacement parameters refined to larger values, suggesting static disorder on these sites. Atomic displacement parameters on O4*a*–O5*a* were constrained to be equal and their positions refined, resulting in a distorted octahedron around W2. In

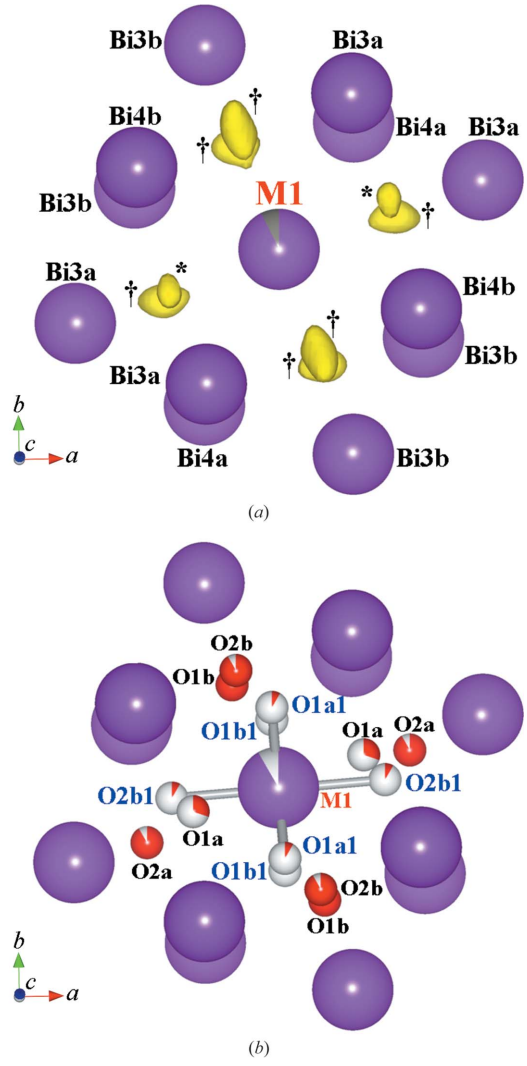

Figure 2
Observed Fourier maps of $Bi_{8.2}WO_{15.3}$ in the vicinity of the mixed *M*1 site. Nearest-neighbour cation sites are shown. Bi is purple, W is gray, O is red (fractional occupancies are denoted by full sectors). (*a*) Positive Fourier peaks around *M*1 are yellow. Peaks marked * are relatively isotropic and correspond to fluorite-type positions, while peaks marked † are relatively irregular and suggestive of split sites. (*b*) The refined oxygen positions and occupancies around the *M*1 site in the same projection. Bonds are drawn to highlight $W1O_6$ octahedra.

Table 2
Crystal and refinement details.

Crystal data			
Composition	$Bi_{35.66}W_{4.34}O_{66.51}$		
Crystal system, space group	Tetragonal, $I4_1$		
Temperature (K)	298		
a, c (Å)	12.5576 (4), 11.2740 (7)		
Z	1		
V (Å^3)	1777.8 (1)		
Data collection			
Radiation type	Synchrotron, λ = 0.41328	Neutron, λ = 0.8–5.2	Combined
Crystal size (μm^3)	∼ 125	12.2	
Crystal color/shape	Transparent yellow prism		
hkl range	$-26 \le h \le 16$, $-27 \le k \le 24$, $-24 \le l \le 16$	$-19 \le h \le 19$, $-19 \le k \le 19$, $-17 \le l \le 17$†	
θ range (°)	1.33–26.81	3.72–70.67	
No. of measured reflections	31 554	15 607	47 161
No. of reflections with $I > 3\sigma(I)$ (X-ray data are also averaged)	4042	7715	11 757
Merging R factor	0.0806	–	
Refinement			
No. of parameters	71	71	72
No. of constraints	7	7	7
R_{all}/R	0.2223/0.1223	0.2760/0.1800	0.2709/0.1738
wR_{all}/wR_{obs}	0.1636/0.1532	0.2276/0.2228	0.2210/0.2157
χ^2	2.75	6.37	4.62

† VIVALDI dataset is not complete within the quoted range.

order to prevent over-parameterization of the refinement, the distorted octahedron was constrained to a chemically ideal octahedron with 1.92 Å W^{6+}—O bonds (Brese & O'Keeffe, 1991). This rigid body ($W2O_6$) was defined with W2 as the central atom. Since W2 is located on a 4*a* site, the corresponding rigid body was refined with respect to a translation along z and a rotation about φ. The φ rotation is the rotation of the octahedral unit in the *ab* plane about the *c* axis. These were the only translations and rotations of the $W2O_6$ unit allowed by site symmetry. Comparing the constrained octahedron against the unconstrained octahedron, negligible increases in R factors were observed.

The final, and most difficult, parts of the structure to refine were the overlapping octahedral and cubic coordination environments (containing 14 partially occupied O sites around *M*1). The Fourier difference map of the region around *M*1 is shown in Fig. 2(*a*). Eight peaks are clearly seen, corresponding to the eight fluorite-type oxygen positions around the *M*1 site. Six of these peaks (labeled † in Fig. 2*a*) are quite anisotropic, elongated towards *M*1. The other two (labeled * in Fig. 2*a*) are relatively isotropic and noticeably weaker. The six elongated peaks suggest split oxygen sites, in which one O atom is closer to *M*1 and the other further away. Two sets of O atoms were therefore introduced: eight fluorite-type O atoms corresponding to the eightfold average coordination expected for Bi; six O atoms corresponding to the octahedral sixfold coordination expected for W. Fig. 2(*b*) highlights the refined $W1O_6$ octahedron by drawing W—O bonds, while leaving the fluorite-related O atoms as non-bonded atoms.

Having defined the complex coordination environments of *M*1, we refined it against combined X-ray and neutron diffraction data. Positions of the fluorite-type O atoms (O1*a*, O1*b*, O2*a* and O2*b*) were refined freely, while positions of atoms in WO_6 (W1, O1*a*1, O1*b*1 and O2*b*1) were refined as a rigid body in the same manner as described above for $W2O_6$. Again, the central atom (W1) of the WO_6 unit is located on a 4*a* position, thus only z translation and φ rotation were refined for the rigid body. Isotropic atomic displacement parameters for O atoms within the two groups were constrained to be equal and refined. These variables were refined in parallel with the refinement of the Bi:W ratio on *M*1, and this ratio was linked to the occupancies of the O atoms surrounding it, *i.e.* the occupancies of the O atoms forming the WO_6 octahedron (O1*a*1, O1*b*1 and O2*b*1) were tied to the W fraction on *M*1, while the occupancies of the fluorite-type O atoms (O1*a*, O1*b*, O2*a* and O2*b*) were tied to the Bi occupancy on *M*1. The refinement converged to a stable minimum. The only remaining significant features in Fourier-difference maps were negative peaks associated with the fluorite-type O1*a* site, indicating reduced occupancy on this site. Free refinement of the O1*a* site occupancy was significantly influenced by the constraint of the atomic displacement parameters to be equal on the fluorite-type O atoms (O1*a*–O2*b*) bonded to *M*1. Thus, the refined Bi:W ratio was used to calculate the stoichiometry of the compound and O1*a* site occupancy adjusted to 0.314 to account for the vacancies. The structure was then refined, resulting in a small displacement of O1*a*, and satisfying the charge-balanced stoichiometry of $Bi_{35.66}W_{4.34}O_{66.51}$.

Final atomic parameters and bond valence sums (BVS) (Brese & O'Keeffe, 1991) are given in Table 1, crystal details in Table 2, and selected bond lengths in Table 3.[1] The structural model is shown in Figs. 3(*a*) and (*b*) highlighting the different *M*1 environments. The refined composition is $Bi_{35.66}W_{4.34}O_{66.51}$ (or $Bi_{8.2}WO_{15.3}$), slightly Bi-rich in comparison to the composition determined by EDS [Bi:W = 6.1(3):1], the initial input Bi:W ratio, and the Bi:W ratios determined from cation-only refinements of either the single-crystal synchrotron X-ray data or single-crystal neutron and synchrotron X-ray data (7.86:1 and 7.98:1, respectively).

[1] Supplementary data for this paper are available from the IUCr electronic archives (Reference: BP5029). Services for accessing these data are described at the back of the journal.

Table 3
Selected metal–oxygen bond lengths in the refined structure of $Bi_{8.2}WO_{15.3}$.

The bonds involved in WO_6 octahedra are marked with asterisks.

Bi1—O1*a*	1.899 (9) ×2	Bi4*a*—O1*b*	2.756 (5)
Bi1—O1*b*	2.384 (4) ×2	Bi4*a*—O2*a*	2.162 (4)
Bi1—O2*b*	2.718 (4) ×2	Bi4*a*—O1*b*1	2.152 (18)*
Bi1—O2*a*	3.195 (4) ×2	Bi4*a*—O3*a*	2.170 (6)
W1—O1*a*1	1.92 (4)* ×2	Bi4*a*—O3*a*	2.166 (6)
W1—O1*b*1	1.92 (4)* ×2	Bi4*a*—O4*a*	3.182 (7)*
W1—O2*b*1	1.92* ×2	Bi4*a*—O4*a*	2.382 (2)*
W2—O4*a*	1.92* ×2	Bi4*a*—O5*a*	3.229 (4)*
W2—O4*b*	1.920 (6)* ×2	Bi4*b*—O1*a*	2.720 (10)
W2—O5*a*	1.920 (6)* ×2	Bi4*b*—O2*b*	2.185 (5)
Bi3*a*—O1*a*	2.579 (10)	Bi4*b*—O1*a*1	2.99 (2)*
Bi3*a*—O1*a*	2.662 (10)	Bi4*b*—O3*b*	2.202 (7)
Bi3*a*—O2*a*	2.277 (6)	Bi4*b*—O3*b*	2.117 (6)
Bi3*a*—O2*b*	2.367 (4)	Bi4*b*—O4*b*	2.195 (5)*
Bi3*a*—O1*a*1	2.46 (2)*	Bi4*b*—O4*b*	3.096 (4)*
Bi3*a*—O2*b*1	2.118 (2)*	Bi4*b*—O5*a*	3.111 (4)*
Bi3*a*—O3*a*	2.762 (6)		
Bi3*a*—O3*a*	2.490 (5)		
Bi3*a*—O4*a*	3.213 (7)*		
Bi3*a*—O4*b*	3.271 (4)*		
Bi3*b*—O1*b*	2.275 (5)		
Bi3*b*—O1*b*	2.361 (5)		
Bi3*b*—O2*a*	2.250 (4)		
Bi3*b*—O2*b*	2.283 (5)		
Bi3*b*—O1*a*1	2.715 (11)*		
Bi3*b*—O1*b*1	2.676 (12)*		
Bi3*b*—O1*b*1	3.25 (2)*		
Bi3*b*—O2*b*1	2.77 (3)		
Bi3*b*—O3*b*	2.936 (7)		
Bi3*b*—O3*b*	2.408 (5)		
Bi3*b*—O5*a*	2.472 (6)*		

The large *R* factors resulting from the structural refinements (Table 2) suggest high levels of disorder, especially in the oxygen sublattice at this composition. It is unlikely that higher-quality data would improve these statistics as the disorder seems to be an inherent property of the material and correlates with the oxide-ion conductivity measurements (Watanabe & Ono, 2004). High *R* factors from refinements against single-crystal data are shown in many materials based on δ-Bi_2O_3 exhibiting high oxide-ion conductivity, such as $Bi_{38}Mo_7O_{78}$ with $wR_I = 0.2167$ at room temperature (Sharma *et al.*, 2009). It should also be noted that the *R* factors available in the literature obtained from refinements against VIVALDI data tend to be higher then the *R* factors obtained from X-ray studies (*e.g.* for $AlF_3{\cdot}9H_2O$, X-ray $wR_2 = 0.048$, while VIVALDI $wR_2 = 0.135$; Kemnitz *et al.*, 2006). This is predominantly attributed to factors such as limited beam time, which in turn limits the ability to collect multiple datasets to improve merging statistics (*e.g.* for $C_{20}H_{30}Zn$, synchrotron X-ray $R_{int} = 5.4\%$, while VIVALDI $R_{int} = 36.4\%$; Van der Maelen *et al.*, 2007). The difficulty in testing crystal quality prior to undertaking experiments and the crystal volumes used are often near the lower limit of what is feasible by neutron diffraction. The crystallographic detail being investigated on VIVALDI, *e.g.* H atoms (Yousufuddin *et al.*, 2005; Van der Maelen *et al.*, 2007) may warrant higher statistics, but this detail is not well determined by X-ray methods. The instrumental and data-reduction aspects, in particular the uncorrected systematic errors introduced by the wide waveband used in the Laue neutron technique, do influence the reported *R* factors. Furthermore, the majority of the published data from VIVALDI is based on small molecule crystallography rather than the solid-state/metal-oxide crystallography (Turner *et al.*, 2005; Ding *et al.*, 2005; Troyanov *et al.*, 2004; Yousufuddin *et al.*, 2005; Van der Maelen *et al.*, 2007; Kemnitz *et al.*, 2006). However, when time is not a limiting factor R_F values near 0.05 can be achieved (Turner *et al.*, 2005) with the wavelength-dependent errors absorbed by the high data redundancy. Since our data collection was not limited by time, and there was a high degree of redundancy, due to the tetragonal symmetry and large number of Laue patterns, the high *R* factors for the neutron part of the refinement must be due to inherent disorder. Note also that the *R* factors on the X-ray part are also high. Nonetheless, this work presents the first simultaneous refinement of a δ-Bi_2O_3-type structure against

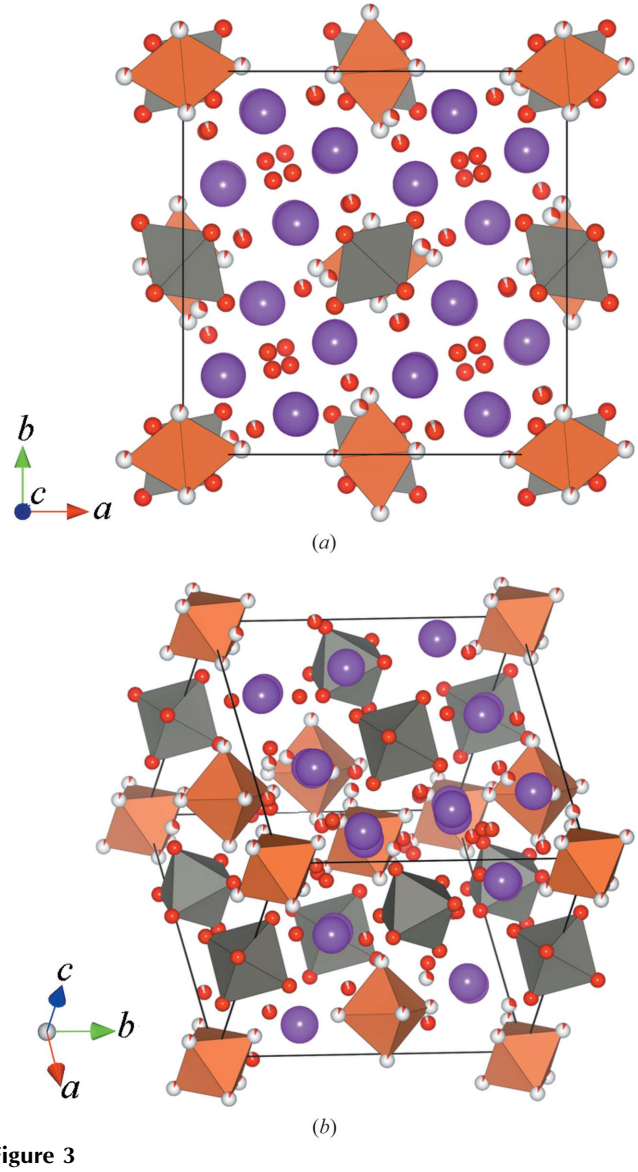

Figure 3
The refined crystal structure of $Bi_{8.2}WO_{15.3}$ viewed along the (*a*) [001] and (*b*) F directions. The latter is a projection along a fluorite-type or δ-Bi_2O_3-type direction in the structure of $Bi_{8.2}WO_{15.3}$. Bi is purple, O is red, $W1O_6$ octahedra are orange, and $W2O_6$ octahedra are light gray.

synchrotron X-ray single-crystal and neutron single-crystal diffraction data.

3.3. Structural features

The calculated BVS presented in Table 1 show reasonable agreement with expected values, with only a few discrepancies. These discrepancies are predominantly due to the ordering of O atoms around W^{6+}, which have much more directional bonding requirements than Bi^{3+}. The most extreme case is Bi3*a*, which is underbonded when BVS are calculated for the average structure because its coordination environment includes the partially occupied oxygen sites O1*a*, O2*a*, O2*b*, O1*a*1 and O2*b*1 (the closest contact to *M*3*a*). Locally, however, all of these oxygen sites must be either fully occupied or fully vacant, depending on the local identity of the mixed *M*1 site to which they coordinate. The average BVS for Bi3*a* represents a compromise between underbonding when *M*1 is Bi1, and overbonding when *M*1 is W1. For the same reason, O atoms show good BVS with the exception of those bonded to W, which are slightly overbonded because the formation of WO_6 octahedra involves moving some O atoms closer to Bi sites than would normally occur in the average fluorite-type structure. Nevertheless, the shortest refined Bi—O distance is 1.899 (9) Å (to the partially occupied O1*a* site), and all others are longer than 2.1 Å, which is comparable to the shortest Bi—O distances in other transition-metal-doped superstructures based on δ-Bi_2O_3 [*e.g.* 2.03 (3) Å in $Bi_{38}Mo_7O_{78}$ (Sharma *et al.*, 2009) and 2.086 (3) Å in $Bi_{14}ReO_{24.5}$ (Crumpton *et al.*, 2005)]. The Bi1–O1*a* distance is particularly short due to the refinement compensating for the constrained atomic displacement parameter on the O1*a* site in addition to the reduced occupancy on this site. It was necessary to maintain the constrained atomic displacement parameter for O1*a* as it was part of the fluorite-related sites bonded to Bi1. Note that we have considered the possibility of applying a high resolution total scattering approach with pair distribution function (PDF) analysis to further probe the local bonding (especially Bi—O) in this model. However, in this case it is likely that the large number of similar Bi—O bond distances would simply result in a single broad peak at low *R*.

The large atomic displacement parameters on O4*a*—O5*a* can be accounted for by introducing split sites. This process occurred in the description of the structure of δ-Bi_2O_3, where the average δ-Bi_2O_3 structure was found to be more correctly modeled by introducing split oxygen sites (Battle *et al.*, 1983). However, in our case the statistical gain in introducing split sites for O4*a*—O5*a* would not merit the increase in the number parameters. Fig. 3(*a*) shows that WO_6 units on W2 and the mixed-cation site *M*1 form chains along [001]. Although the W sites are not nearest-neighbor cations in this (or any other) direction, these [001] chains do also contain oxygen vacancies (on the O1*a* site) and the largest refined atomic displacement parameters of all O atoms (on the O4*a*–O5*a* sites), which may be indicative of static disorder. These channels may therefore be responsible for the high levels of oxide-ionic conductivity observed in the type (Ib) solid solution in the Bi_2O_3–WO_3 system.

4. Conclusions

A structural model for the composition $Bi_{35.66}W_{4.34}O_{66.51}$ in the type (Ib) solid solution of the Bi_2O_3–W_2O_6 system has been determined and refined simultaneously against single-crystal neutron and synchrotron X-ray diffraction data. Refinement against only the X-ray dataset resulted in poor precision on the O sublattice, while refinement against only neutron data reduced the accuracy on cation positions compared with X-ray data and led to unreasonable atomic displacement parameters on the cations. Therefore, to overcome these shortfalls, this work reports the first simultaneous refinement of a transition-metal doped δ-Bi_2O_3-type structure from single-crystal neutron and synchrotron X-ray diffraction data. The single crystal was grown by the floating-zone furnace method and was found to adopt tetragonal $I4_1$ space-group symmetry. This work also presents the first attempt to refine fully the oxygen sublattice in the type (Ib) solid solution. We use crystal-chemical considerations to propose an octahedral local coordination environment of W-containing sites, which is confirmed by crystallographic evidence in collected data. Careful analysis of the combined X-ray and neutron datasets shows the existence of a mixed Bi/W site with dual coordination environments and oxygen vacancies. These parameters were modelled and refined. The resulting large *R* factors of the refinements agree with the notion of disorder in the oxygen sublattice, shown by earlier conductivity measurements. This disorder also limits full unconstrained refinements of the structural model. Our analysis of this compound illustrates the difficulties associated with trying to understand structural properties of disordered, but highly conducting, materials.

This work was supported by the Australian Research Council – Discovery Projects (DP0666465) and the Australian Institute of Nuclear Science and Engineering Postgraduate Research Awards scheme. Collection of synchrotron X-ray diffraction data at the Advanced Photon Source was supported by the Australian Synchrotron Research Program, which is funded by the Commonwealth of Australia under the Access to Major Research Facilities Programme. Use of the Advanced Photon Source is supported by the US Department of Energy, Office of Science, Office of Basic Energy Sciences, under Contract No. DE-AC02-06CH11357. Financial support for travel to the ILL was provided by the Access to Major Research Facilities Programme which is a component of the International Science Linkages Programme established under the Australian Government's innovation statement, Backing Australia's Ability.

References

Battle, P. D., Catlow, C. R. A., Drennan, J. & Murray, A. D. (1983). *J. Phys. Solid State Phys.* **16**, L561–L566.
Boivin, J. C. & Mairesse, G. (1998). *Chem. Mater.* **10**, 2870–2888.

Brese, N. E. & O'Keeffe, M. (1991). *Acta Cryst.* B**47**, 192–197.
Bruker AXS (2001*a*). *SADABS*, Version 2.03. Bruker AXS Inc., Madison, Wisconsin, USA.
Bruker AXS (2001*b*). *SAINTPlus*, Version 6.45. Bruker AXS Inc., Madison, Wisconsin, USA.
Campbell, J. W. (1995). *J. Appl. Cryst.* **28**, 228–236.
Campbell, J. W., Habash, J., Helliwell, J. R. & Moffat, K. (1986). *Inf. Q. Protein Crystallogr.* **18**, 23–31.
Campbell, J. W., Hao, Q., Harding, M. M., Nguti, N. D. & Wilkinson, C. (1998). *J. Appl. Cryst.* **31**, 496–502.
Cheetham, A. K. & Rae Smith, A. R. (1985). *Acta Cryst.* B**41**, 225–230.
Crumpton, T. E., Francesconi, M. G. & Greaves, C. (2003). *J. Solid State Chem.* **175**, 197–206.
Crumpton, T. E., Mosselmans, J. F. W. & Greaves, C. (2005). *J. Mater. Chem.* **15**, 164–167.
Ding, E., Du, B., Meyers, E. A., Shore, S. G., Yousufuddin, M., Bau, R. & McIntyre, G. J. (2005). *Inorg. Chem.* **44**, 2459–2464.
Farrugia, L. J. (1999). *J. Appl. Cryst.* **32**, 837–838.
Francesconi, M. G., Kirbyshire, A. L., Greaves, C., Richard, O. & Van Tendeloo, G. (1998). *Chem. Mater.* **10**, 626–632.
Gattow, G. & Schröder, H. (1962). *Z. Anorg. Allg. Chem.* **318**, 176–189.
Hoda, S. N. & Chang, L. L. Y. (1974). *J. Am. Ceram. Soc.* **57**, 323–326.
Kemnitz, E., Gros, U., Rüdiger, S., Scholz, G., Heidemann, D., Troyanov, S. I., Morosov, I. V. & Lemée-Cailleau, M. H. (2006). *Solid State Sci.* **8**, 1443–1452.
Ling, C. D. (1999). *J. Solid State Chem.* **148**, 380–405.
Ling, C. D. (2006). *Physica B*, **385–386**, 193–195.
Ling, C. D., Withers, R. L., Schmid, S. & Thompson, J. G. (1998). *J. Solid State Chem.* **137**, 42–61.
Ling, C. D., Withers, R. L., Thompson, J. G. & Schmid, S. (1999). *Acta Cryst.* B**55**, 306–312.
Liu, Y. H., Li, J. B., Liang, J. K., Luo, J., Ji, L. N., Zhang, J. Y. & Rao, G. H. (2008). *Mater. Chem. Phys.* **112**, 239–243.
McDowell, N. A., Knight, K. S. & Lightfoot, P. (2006). *Chem. Eur. J.* **12**, 1493–1499.
McIntyre, G. J., Lemée-Cailleau, M. H. & Wilkinson, C. (2006). *Physica B*, **385–386**, 1055–1058.
Nespolo, M., Watanabe, A. & Suetsugu, Y. (2002). *Cryst. Res. Technol.* **37**, 414–422.
Petricek, V., Dusek, M. & Palatinus, L. (2007). *JANA*2006. Institute of Physics, Prague, Czech Republic.
Rae, A. D., Thompson, J. G. & Withers, R. L. (1991). *Acta Cryst.* B**47**, 870–881.
Sammes, N. M., Tompsett, G. A., Nafe, H. & Aldinger, F. (1999). *J. Eur. Ceram. Soc.* **19**, 1801–1826.
Sharma, N., Macquart, R. B., Christensen, M., Avdeev, M., Chen, Y.-S. & Ling, C. D. (2009). *J. Solid State Chem.* **182**, 1312–1318.
Sheldrick, G. M. (2008). *Acta Cryst.* A**64**, 112–122.
Spinolo, G. & Tomasi, C. (1997). *Powder Diffr.* **12**, 16–19.
Takahashi, T. & Iwahara, H. (1973). *J. Appl. Electrochem.* **3**, 65–72.
Troyanov, S. I., Morozov, I. V., Snigireva, E. M., Ling, C. D. & Kemnitz, E. (2004). *J. Solid State Chem.* **177**, 3224–3228.
Turner, D. R., Henry, M., Wilkinson, C., McIntyre, G. J., Mason, S. A., Goeta, A. E. & Steed, J. W. (2005). *J. Am. Ceram. Soc.* **127**, 11063–11074.
Van der Maelen, J. F., Gutiérrez-Puebla, E., Monge, Á., García-Granda, S., Resa, I., Carmona, E., Fernández-Díaz, M. T., McIntyre, G. J., Pattison, P. & Weber, H.-P. (2007). *Acta Cryst.* B**63**, 862–868.
Watanabe, A., Ishizawa, N. & Kato, M. (1985). *J. Solid State Chem.* **60**, 252–257.
Watanabe, A. & Ono, A. (2004). *Solid State Ion.* **174**, 15–18.
Wilkinson, C., Cowan, J. A., Myles, D. A. A., Cipriani, F. & McIntyre, G. J. (2002). *Neutron News*, **13**, 37–41.
Wilkinson, C., Khamis, H. W., Stansfield, R. F. D. & McIntyre, G. J. (1988). *J. Appl. Cryst.* **21**, 471–478.
Wolfe, R. W., Newnham, R. E. & Kay, M. I. (1969). *Solid State Commun.* **7**, 1797–1801.
Yousufuddin, M., Wen, T. B., Mason, S. A., McIntyre, G. J., Jia, G. & Bau, R. (2005). *Angew. Chem. Int. Ed.* **44**, 7227–7230.
Zhou, W. (1994). *J. Solid State Chem.* **108**, 381–394.